Draft version November 16, 2009
Preprint typeset using LaTeX style emulateapj v. 08/22/09

arXiv:0911.3146v1 [astro-ph.HE] 16 Nov 2009

A *CHANDRA X-RAY OBSERVATORY* STUDY OF PSR J1740–5340 AND CANDIDATE MILLISECOND PULSARS IN THE GLOBULAR CLUSTER NGC 6397

Slavko Bogdanov[1,2], Maureen van den Berg[3], Craig O. Heinke[4], Haldan N. Cohn[5], Phyllis M. Lugger[5], Jonathan E. Grindlay[3]

Draft version November 16, 2009

ABSTRACT

We present a deep *Chandra X-ray Observatory* study of the peculiar binary radio millisecond pulsar PSR J1740–5340 and candidate millisecond pulsars (MSPs) in the globular cluster NGC 6397. The X-rays from PSR J1740–5340 appear to be non-thermal and exhibit variability at the binary period. These properties suggest the presence of a relativistic intrabinary shock formed due to interaction of a relativistic rotation-powered pulsar wind and outflow from the unusual "red-straggler/sub-subgiant" companion. We find the X-ray source U18 to show similar X-ray and optical properties to those of PSR J1740–5340, making it a strong MSP candidate. It exhibits variability on timescales from hours to years, also consistent with an intrabinary shock origin of its X-ray emission. The unprecedented depth of the X-ray data allows us to conduct a complete census of MSPs in NGC 6397. Based on the properties of the present sample of X-ray–detected MSPs in the Galaxy we find that NGC 6397 probably hosts no more than 6 MSPs.

Subject headings: globular clusters: general — globular clusters: individual (NGC 6397) — pulsars: general — pulsars: individual (PSR J1740–5340) — stars: neutron — X-rays: stars

1. INTRODUCTION

Globular clusters are well known for their abundance of rotation-powered millisecond pulsars (Camilo et al. 2000; Freire et al. 2003; Ransom et al. 2005)[6]. These objects are believed to have been produced by the evolution of low-mass X-ray binaries (LMXBs) that were themselves produced through dynamical interactions of binaries and neutron stars. The superb sub-arcsecond X-ray imaging capability of the *Chandra X-Ray Observatory* has allowed X-ray studies of MSPs in the dense cores of globular clusters for the first time. In addition to establishing the X-ray properties of the Galactic population of MSPs, X-ray studies of cluster MSPs offer constraints on stellar and binary evolution and the internal dynamical evolution of globular clusters. To date, X-ray counterparts of these systems have been detected with *Chandra* in 47 Tuc (Grindlay et al. 2002; Bogdanov et al. 2006), NGC 6397 (Grindlay et al. 2002, and this work), M28 (Becker et al. 2003, S. Bogdanov et al. in preparation), M4 (Bassa et al. 2004), NGC 6752 (D'Amico et al. 2002), M71 (Elsner et al. 2008), and Ter 5 (Heinke et al. 2006).

NGC 6397 is the nearest apparently core-collapsed and the second closest globular cluster, with $D \approx 2.4$ kpc (Hansen et al. 2007; Strickler et al. 2009, and references therein). It hosts one known MSP, PSR J1740–5340 (D'Amico et al. 2001), which is bound to an unusual "red-straggler" or "sub-subgiant"[7] companion in a 32.5-hour binary orbit (Ferraro et al. 2003). This is at odds with the standard MSP formation theory that predicts either a white dwarf or a very-low-mass ($\sim$0.03 $M_{\odot}$) degenerate companion (see Bhattacharya & van den Heuvel 1991, for a review), implying that either this binary has just emerged from the "recycling" phase in a LMXB (Burderi et al. 2002) or has been involved in a close dynamical binary-binary encounter in which the original companion to the pulsar was exchanged for the current one (Camilo & Rasio 2005, and references therein).

Observations of MSPs, both in the field of the Galaxy and in globular clusters, have revealed that their X-ray emission can be of thermal and/or non-thermal character (see Zavlin 2007; Bogdanov & Grindlay 2008, for a review). In many MSPs, the X-rays appear to be predominantly due to surface emission from the magnetic polar caps of the neutron star (Bogdanov et al. 2006; Zavlin 2006; Bogdanov & Grindlay 2009). Non-thermal pulsed X-ray emission, on the other hand, can arise from particle acceleration processes in the pulsar magnetosphere as seen from the most energetic MSPs (see, e.g. Rutledge et al. 2004). Alternatively, non-thermal X-rays can be produced via interaction of the rotation-powered pulsar wind with the ambient interstellar medium, as seen for PSR B1957+20 (Stappers et al. 2003) and J2124–3358 (Hui & Becker 2006), or material from a close binary companion as in PSR J0024–7204W in 47 Tuc (Bogdanov et al. 2005).

In this paper, we present *Chandra* deep imaging spectroscopic observations of NGC 6397, with a particular fo-

---

[1] Department of Physics, McGill University, 3600 University Street, Montreal, PQ H3A 2T8, Canada; bogdanov@physics.mcgill.ca
[2] Canadian Institute for Advanced Research Junior Fellow
[3] Harvard-Smithsonian Center for Astrophysics, 60 Garden Street, Cambridge, MA 02138, U.S.A.
[4] Department of Physics, University of Alberta, Edmonton, AB T6G 2G7, Canada
[5] Department of Astronomy, Indiana University, 727 East Third Street, Bloomington, IN 470405, U.S.A.

[6] For an up-to-date list of all known globular cluster MSPs see http://www.naic.edu/~pfreire/GCpsr.html.

[7] The terms red straggler and sub-subgiant are used for cluster stars that lie in a location below the base of the red giant branch that is difficult to understand in the context of standard evolution scenarios for single stars or binaries in a dynamically inactive environment (Orosz & van Kerkwijk 2003).

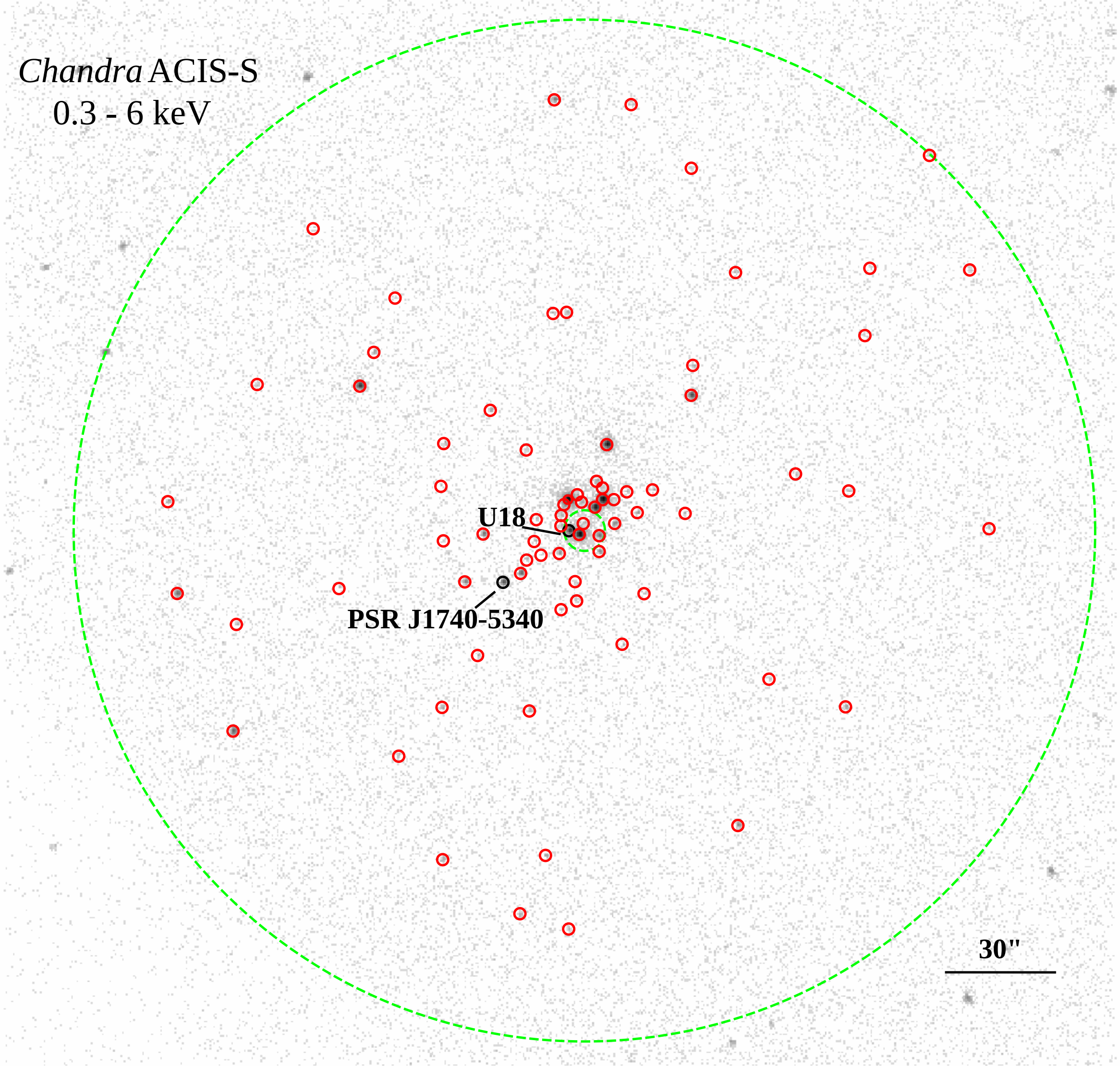

FIG. 1.— Coadded *Chandra X-ray Observatory* 295.1-ks ACIS-S3 image of the core of the globular cluster NGC 6397 in the 0.3–6 keV band. The 1.5″ circles are centered on the 79 X-ray sources detected within the 2.3′ half-mass radius of the cluster (outer dashed circle), with the positions of PSR J1740–5340 (U12) and CXOGlb J174041.6–534027 (U18) marked. The inner dashed circle shows the 5.5″ core radius of the cluster. The grayscale corresponds to number of counts increasing logarithmically from 0 (*white*) to 3515 (*black*). North is up and east is to the left.

cus on PSR J1740–5340 and CXOGlb J174041.6–534027 (U18), a plausible MSP candidate. We also investigate the X-ray source population of NGC 6397 in an attempt to identify plausible MSP candidates and constrain the MSP content of this cluster. The work is organized as follows. In §2 we describe the data reduction and analysis procedures. In §3 we focus on the properties of PSR J1740–5340, while in §4 we investigate the MSP candidate U18. In §5 we attempt to place interesting constraints on the total number of MSPs in the cluster based on the available X-ray and optical data. We present a discussion in §6 and conclusions in §7.

2. DATA REDUCTION AND ANALYSIS

The *Chandra* data discussed herein were acquired during two separate observations in Cycle 8, on 2007 June 22 (ObsID 7461) and 2007 July 16 (ObsID 7460) for 90 and 160 ks, respectively. In both cases the ACIS S3 chip in VFAINT telemetry mode was at the focus. We also make use of two Cycle 3 ACIS-S observations of 28.5 ks and 27 ks (ObsIDs 2668 and 2669, respectively), and a single Cycle 1 ACIS-I (ObsID 79) observation of 49 ks (Grindlay et al. 2001), all acquired in FAINT mode. Table 1 summarizes all the observations used in this work.

The data re-processing, reduction, and analysis were performed using CIAO[8] 4.0. Starting from the level 1 data products, we first removed pixel randomization from the standard pipeline processing in order to aid in source disentanglement in the dense cluster core. In addition, for the purposes of faint source detection we applied the background cleaning algorithm for the data taken in VFAINT observing mode. However, as this procedure tends to discard real source counts for relatively bright

---

[8] Chandra Interactive Analysis of Observations, available at http://cxc.harvard.edu/ciao/

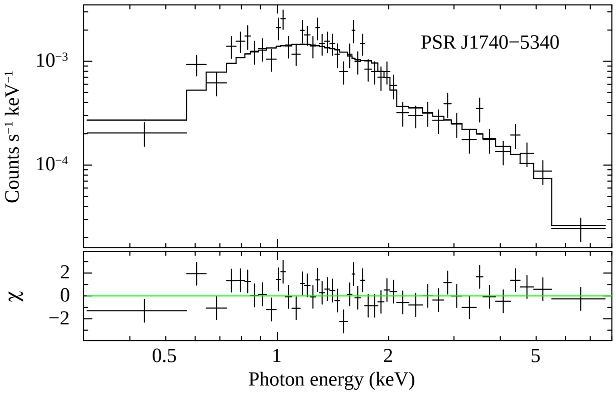

Fig. 2.— Phase-integrated stacked spectrum of PSR J1740–5340 from all four *Chandra* ACIS-S observations, fitted with an absorbed powerlaw spectrum. The lower panel shows the best fit residuals. See the text and Table 2 for the best fit parameters.

sources, the background-cleaned data were not used for the spectral analyses discussed in §3 and §4 but were used for the population study in §5. Before coadding the four ACIS-S images, the individual aspect solutions were reprojected relative to the longest observation (ObsID 7460) using the brightest sources in the cluster in order to correct for any differences in the absolute astrometry between the four exposures.

X-ray source detection was performed with the `wavdetect` tool in CIAO. In the crowded cluster core, we also used the PWDetect[9] script (Damiani et al. 1997a,b), which tends to be more effective at identifying faint sources near much brighter sources. The resulting source positions were refined using the IDL tool `acis_extract`. The 95% confidence positional uncertainty radius for each source was computed using the empirical relation given by Equation (5) in Hong et al. (2005). In total, 79 sources are detected within the 2.33' half-mass radius of NGC 6397 (see Table 3). Compared to the source list from Grindlay et al. (2001), based on the single ACIS-I observation, and Grindlay (2005), based on the ACIS-I and two short ACIS-S observations, we find that all sources except U20, U64, U71, U72, U74, U78, and U85 are detected in the combined deep ACIS-S image.

For the purposes of optical matching of the X-ray sources (see §5) using the set of *Hubble Space Telescope* Advanced Camera for Surveys Wide Field Channel observations (GO-10257) in F435W (B), F625W (R), and F658N (Hα), we computed a boresight correction for the *Chandra* source coordinates (see H. Cohn, in preparation, for details). The resulting shift of the *Chandra* coordinates is $\Delta\alpha = -0.19'' \pm 0.02''$ $\Delta\delta = 0.18'' \pm 0.02''$. The X-ray position based on this correction for PSR J1740–5340 agrees with the optical position (Bassa & Stappers 2004) to 0.01″ in α and 0.03″ in δ. While the *Chandra* ACIS-S mosaic encompasses the entire half-mass radius of the cluster, the *HST* ACS/WFC mosaic provides complete coverage out to a radius of $\sim 1\overset{\prime}{.}5$ from the cluster center, partial coverage in two or more exposures out to $\sim 2\overset{\prime}{.}5$, and partial coverage in at least one exposure out to $2\overset{\prime}{.}9$. As a result, the sources U5, U16, U77, and U84, lie outside the R field making their classification difficult due to the absence of BR and $\mathrm{H}\alpha - R$ color measurements. However, Kaluzny et al. (2006) have shown that the optical counterparts of U5 and U77, V30 and V36 respectively, are variable using ground-based photometry and thus are probably active binaries (Kaluzny et al. 2006).

TABLE 1
Chandra Observations of NGC 6397

Telescope/ Instrument	Epoch of Observation	Observation ID	Exposure Time (ks)
Chandra/ACIS-I	2000 Jul 31	79	49.0
Chandra/ACIS-S	2002 May 13	2668	28.5
Chandra/ACIS-S	2002 May 15	2669	27.0
Chandra/ACIS-S	2007 Jun 22	7461	90.0
Chandra/ACIS-S	2007 Jul 16	7460	160.0

Net counts and spectra for each X-ray source were extracted using `acis_extract` from polygonal regions sized to contain 90% of the total energy at 1.5 keV. For spectroscopy, the extracted source counts in the 0.3–8 keV range were then grouped in energy bins so as to ensure at least 15 counts per bin. The X-ray spectral analyses of PSR J1740–5340 and U18 were carried out using the XSPEC[10] package. For the variability analysis, the photon arrival times were first reduced to the solar system barycenter, using the CIAO tool `axbary`.

3. PSR J1740–5340

Grindlay et al. (2001, 2002) have found the X-ray counterpart of the PSR J1740–5340 system (see Figure 1) to be a moderately luminous ($L_X \sim 10^{31}$ ergs s^{-1}) and relatively hard X-ray source ($\Gamma \sim 1.4$), compared to most MSPs. Indeed, the combined *Chandra* ACIS-S spectrum (Figure 2) is well described by a pure non-thermal model with power-law photon index $\Gamma = 1.73 \pm 0.08$, hydrogen column density of $N_H = (2.19^{+0.22}_{-0.25}) \times 10^{21}$ cm^{-2}, and unabsorbed X-ray flux $F_X = (3.2 \pm 0.4) \times 10^{-14}$ ergs cm^2 s^{-1} (0.3–8 keV) with $\chi^2_\nu = 1.14$ for 42 degrees of freedom. All uncertainties quoted are 1σ. For an assumed distance of 2.4 kpc to NGC 6397, the implied X-ray luminosity in the 0.3–8 keV band is $L_X = 2.2 \times 10^{31}$ ergs s^{-1}.

We also applied a two-temperature thermal (blackbody or H atmosphere) model, which provides a good description of the X-ray spectra of several nearby MSPs (Zavlin 2006; Bogdanov & Grindlay 2009). However, this model fits the phase-averaged spectrum of PSR J1740–5340 poorly. The spectrum of PSR J1740–5340 likely contains a soft thermal component (with $T_{\rm eff} \sim 10^6$ K and L_X of order a few$\times 10^{30}$ ergs s^{-1}) originating from the hot magnetic polar caps of the MSP, as seen in many X-ray–detected MSPs (e.g. PSR J0437–4715 and most MSPs in 47 Tuc, see Zavlin 2006; Bogdanov et al. 2006). To investigate this possibility, we first introduce a single blackbody component to the spectral model. Fitting a composite powerlaw plus blackbody model yields $\Gamma = 1.56^{+0.18}_{-0.23}$, $N_{\rm H} = (2.6^{+1.8}_{-0.8}) \times 10^{21}$ cm^{-2}, $kT = 0.19^{+0.09}_{0.04}$ K, and $R_{\rm eff} = 0.15^{+0.09}_{-0.13}$ km with $\chi^2_\nu = 1.1$ for 40 degrees of freedom. Although an F-test indicates that the addition of a thermal component is not statistically warranted by the data, the best fit values for $T_{\rm eff}$ and $R_{\rm eff}$ are similar to those obtained for the 47 Tuc MSPs so this component may in fact be genuine. A composite model consisting of a powerlaw plus two thermal components yields good fits to the spectrum, although the limited photon statistics do not allow meanigful constraints for a three-component model. In principle, the presence of surface thermal emission could be determined by way of high time-resolution X-ray observations, which would reveal any thermal pulsations. Unfortunately, the 3.2-second time resolution of the ACIS observations precludes such an investigation with the present dataset.

---

[9] PWDetect has been developed by scientists at Osservatorio Astronomico di Palermo G. S. Vaiana thanks to Italian CNAA and MURST (COFIN) grants.

[10] Available at http://heasarc.nasa.gov/docs/xanadu/xspec/index.html

The X-ray emission from the PSR J1740–5340 system could also originate from a thermal plasma within the binary, possibly from the active corona of the secondary star or the material responsible for the radio eclipses. To test this possibility, we used the `vmekal` thermal plasma model in XSPEC, with metal abundances set to values representative of the stars in NGC 6397 (Castilho et al. 2000; Gratton et al. 2001). This model also reproduces the observed spectral shape rather well, with best fit parameters $N_{\rm H} = (1.80^{+0.25}_{-0.21}) \times 10^{21}$ cm^{-2}, $kT = 6.2^{+1.4}_{-1.1}$ keV, and $F_X = (2.70^{+0.29}_{-0.36}) \times 10^{-14}$ ergs cm^2 s^{-1} (0.3–8 keV), with $\chi^2_\nu = 1.2$ for 47 degrees of freedom. As discussed in §6.1, although a thermal plasma model is consistent with the observed X-ray emission from the PSR J1740–5340 binary, a predominantly non-thermal origin of the X-rays is more likely.

Based on the ACIS-I observation of NGC 6397, Grindlay et al. (2002) reported evidence for a gradual increase (by a factor of 2 in total) in the X-ray count rate of PSR J1740–5340. However, due to the limited phase coverage and photon statistics, no conclusive statements could be made regarding variability. Figure 3 shows the X-ray count rate from the pulsar as a function of binary phase, based on the radio timing ephemeris from D'Amico et al. (2001), of all *Chandra* observations of PSR J1740–5340. Although the individual lightcurves are suggestive of flux modulations, with generally lower count rates around the radio eclipse phases (0.05–0.45), a Kolmogorov-Smirnov (K-S) test on the unbinned lightcurves within each observation reveals no statistically significant variability. In addition, the same test indicates variability only at a 1.7σ confidence level over the entire set of ACIS-S observations. On the other hand, based on Poisson statistics, we find that the count rate minimum that occurs near $\phi = 0.25$ (see bottom panel of Fig. 3) for the lightcurve folded at the binary period and grouped in 20–40 bins, deviates by $\sim 3.8\sigma$ from what is expected from a constant source. A χ^2 test on the same lightcurve indicates a 98.7% probability of variability. There is also marginal evidence (at ~95% confidence) for spectral variability, with an apparent softening of the X-ray emission around $\phi = 0.25$. Due to the long binary period, the ACIS-S data cover less than 3 full binary orbits so it is not clear whether this variability is truly periodic and stable over many orbits. Interestingly, the folded lightcurve exhibits the same characteristic shape as that of PSR J0024–7204W in 47 Tuc (Bogdanov et al. 2005), with a minimum around superior conjunction, roughly coincident with the radio eclipses. The spectral and temporal similarities of the two systems point to an intrabinary shock origin of the X-rays from PSR J1740–5340.

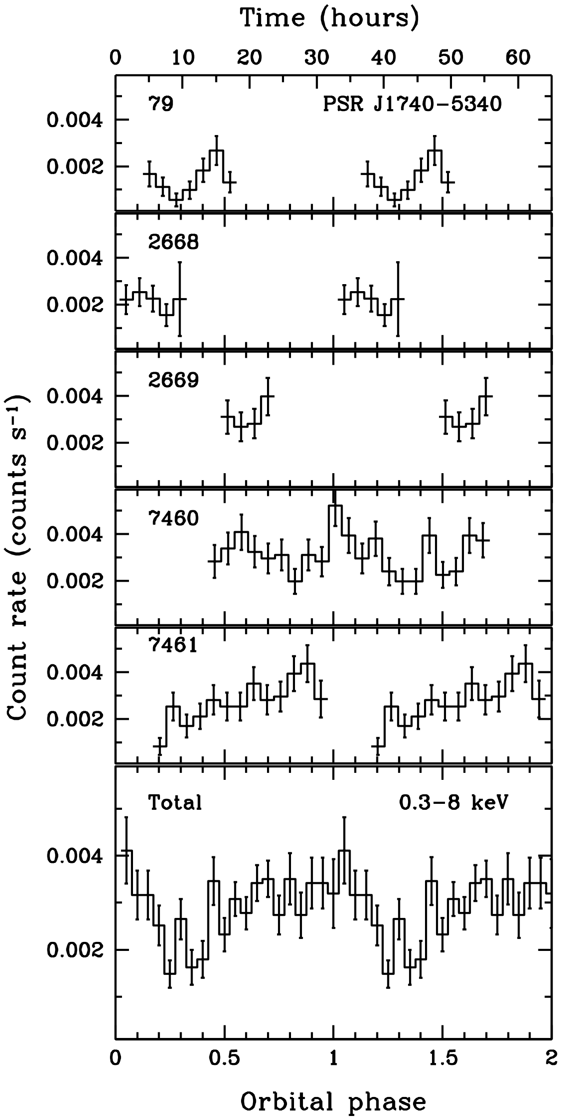

FIG. 3.— Lightcurves of PSR J1740–5340 folded at the pulsar's binary period for each *Chandra* ACIS observation. The bottom panel shows the combined folded lightcurve from the four ACIS-S observations, with the count rate corrected for the non-uniform exposure across the orbit. The phase is defined based on the radio pulsar timing convention in which superior conjunction occurs at $\phi = 0.25$. Two orbital cycles are shown for clarity.

4. U18: A MILLISECOND PULSAR CANDIDATE

The X-ray source CXOGlb J174041.6–534027 (hereafter U18) is positionally coincident with a peculiar "red-straggler" star[11] (Grindlay et al. 2001). In addition, it is known to have a relatively hard spectrum making it a plausible candidate for a MSP given the similarities in X-ray and optical properties with PSR J1740–5340. A

---

[11] We note that the proper motions of the optical counterparts to U12 and U18 are consistent with cluster membership (see H. Cohn, et al., in preparation). Therefore, their anomalous locations in the cluster optical color-magnitude diagram cannot be explained by them being foreground or background objects.

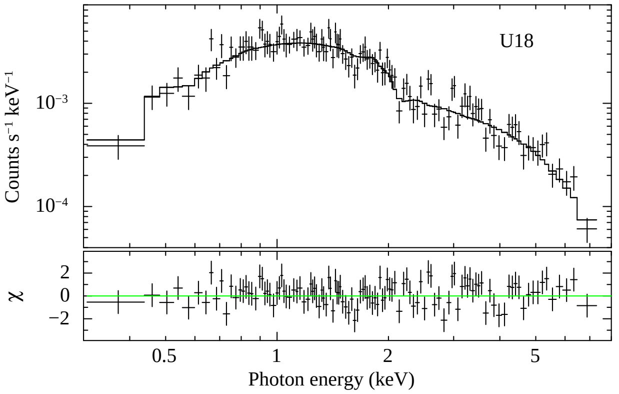

FIG. 4.— Total *Chandra* ACIS-S spectrum of the X-ray source CXOGlb J174041.6–534027 (U18) fitted with a pure powerlaw spectrum. The bottom panel shows the best fit residuals. See text and Table 2 for best fit parameters.

TABLE 2
SPECTRAL FITS FOR PSR J1740–5340 AND U18

Parameter	PSR J1740–5340 (U12)	CXOGlb J174041.7–534027 (U18)
Powerlaw		
$N_{\rm H}$ (10^{21} cm^{-2})	$2.19^{+0.22}_{-0.25}$	$1.40^{+0.12}_{-0.11}$
Γ	$1.73^{+0.08}_{-0.08}$	$1.38^{+0.05}_{-0.04}$
F_X[a] (0.3–8 keV)	$3.22^{+0.37}_{-0.36}$	$9.72^{+0.07}_{-0.02}$
χ^2_ν/dof	1.14/42	1.00/114
Powerlaw+Blackbody		
$N_{\rm H}$ (10^{21} cm^{-2})	$2.58^{+1.80}_{-0.80}$	$1.70^{+0.05}_{-0.07}$
Γ	$1.56^{+0.18}_{-0.23}$	$1.29^{+0.05}_{-0.12}$
kT (keV)	$0.19^{+0.09}_{-0.04}$	$0.19^{+0.03}_{-0.03}$
$R_{\rm eff}$[b] (km)	$0.15^{+0.09}_{-0.13}$	$0.18^{+0.13}_{-0.14}$
F_X[a] (0.3–8 keV)	$3.47^{+0.39}_{-1.66}$	$10.71^{+0.08}_{-0.03}$
χ^2_ν/dof	1.11/40	0.98/112
VMEKAL		
$N_{\rm H}$(10^{21} cm^{-2})	$1.80^{+0.25}_{-0.21}$	$1.53^{+0.14}_{-0.13}$
kT (keV)	$6.2^{+1.4}_{-1.1}$	$16.8^{+4.7}_{-3.4}$
F_X[a] (0.3–8 keV)	$2.70^{+0.29}_{-0.36}$	$9.04^{+0.57}_{-0.71}$
χ^2_ν/dof	1.19/47	1.06/128

[a] Unabsorbed flux in units of 10^{-14} ergs cm^{-2} s^{-1} in the 0.3–8 keV band.

[b] Effective blackbody emission radius assuming a distance of 2.4 kpc to NGC 6397.

fit of a power-law model to the combined ACIS-S spectrum of U18 gives $\Gamma = 1.38^{+0.05}_{-0.04}$, $N_H = (1.4^{+0.12}_{-0.11}) \times 10^{21}$ cm^{-2} with $\chi^2_\nu = 1.0$ for 114 degrees of freedom. The derived unabsorbed flux of $F_X = 9.7 \times 10^{-14}$ ergs cm^{-2} s^{-1} (0.3–8 keV) implies a luminosity of $L_X = 6.7 \times 10^{31}$ ergs s^{-1} for $D = 2.4$ kpc. Figure 4 shows the spectrum of U18 in the 0.3–8 keV band and the best fit PL model.

As with PSR J1740–5340, we also conducted fits using a two component (thermal plus non-thermal) model. The resulting best fit values are $\Gamma = 1.29^{+0.05}_{-0.12}$, $kT = 0.19^{+0.03}_{-0.03}$ keV, $R_{\rm eff} = 0.18^{+0.13}_{-0.14}$, $N_H = (1.70^{+0.05}_{-0.07}) \times 10^{21}$ cm^{-2}, with $\chi^2_\nu = 0.98$ for 112 degrees of freedom. The unabsorbed flux in the 0.3–8 keV band is 1.07×10^{-13} ergs cm^{-2} s^{-1}, which corresponds to an X-ray luminosity of $L_X = 7.4 \times 10^{31}$ ergs s^{-1} for $D = 2.4$ kpc. By analogy with the nearest known MSPs (Zavlin 2006; Bogdanov & Grindlay 2009), we also apply a model with a powerlaw plus two thermal components. This model is consistent with the observed spectrum as well, although the relatively high column density along the line of sight, which absorbs a large fraction of source photons below ∼0.5 keV, makes it difficult to reliably constrain the softer thermal component.

A thermal plasma model (`vmekal` with the same assumed abundances as for PSR J1740–5340) also provides a good description of the spectrum of U18. The best fit parameters in this case are $N_H = (1.53^{+0.14}_{-0.13}) \times 10^{21}$ cm^{-2}, $kT = 16.8^{+4.7}_{-3.4}$ keV, and $F_X = 9.0 \times 10^{-14}$ ergs cm^{-2} s^{-1} (0.3–8 keV), with $\chi^2_\nu = 1.06$ for 128 degrees of freedom.

It is obvious from Figure 5 that the X-ray flux from U18 exhibits variability by as much as a factor of ∼4 on timescales spanning from hours to years. Indeed, a K-S test on the concatenated set of ACIS-S observations indicates a 3.5×10^{-15} probability of the observed photons coming from a steady flux distribution. Moreover, the photon arrival times from U18 within observations 2668, 2669, 7460, and 7461 deviate by 3σ, 2.3σ , 3σ, and 4σ from a constant distribution, based on a K-S test.

Kaluzny et al. (2006) have reported the likely detection of periodicity, possibly due to ellipsoidal variations, with $P = 1.3$ days in the source V31, which they associate with U18. It should be noted, however, that the position of V31 lies at $\sim 2.1\sigma$ from U18 after boresight correction. Moreover, V31 does not correspond to the red-straggler optical counterpart of U18 reported by Grindlay et al. (2001), which is only $\sim 0.4\sigma$ away. We have folded the set of four *Chandra* ACIS-S observations at the period of V31 but find no statistically significant variability. This implies that V31 is most likely not the actual optical counterpart of U18.

5. AN X-RAY CENSUS OF MILLISECOND PULSARS IN NGC 6397

As noted previously, several nearby MSPs in the field of the Galaxy (Zavlin 2006; Bogdanov & Grindlay 2009) and most MSPs in the globular cluster 47 Tuc (Bogdanov et al. 2006) appear to be predominantly soft, thermal X-ray sources due to their hot polar caps. As demonstrated by Bogdanov et al. (2008) (see in particular their Figure 1), the (nearly) antipodal geometry of the polar caps and the effects of light bending guarantee that this surface emission is observed for any combination of magnetic inclinations and viewing angles. In addition, the difference in observed luminosity between the most and least favorable geometric orientations (always face-on versus always edge-on hot spots) is only a factor of ∼3 as a consequence of gravitational bending of light near the neutron star surface. Thus, thermal MSPs should be observable in X-rays even if they cannot be seen in the radio due to unfavorable beaming and fall within a relatively narrow range of X-ray luminosities. The limiting sensitivity of the available ACIS-S data is $\sim 10^{29}$ ergs s^{-1}, meaning that typical thermal MSPs (with luminosities of a few $\times 10^{30}$ ergs s^{-1}) would be detected in the combined *Chandra* ACIS-S observations if they were located in NGC 6397, even in the unlikely event that their two hot spots are always seen edge-on. Binary MSPs that eclipse in the radio tend to have X-ray luminosities

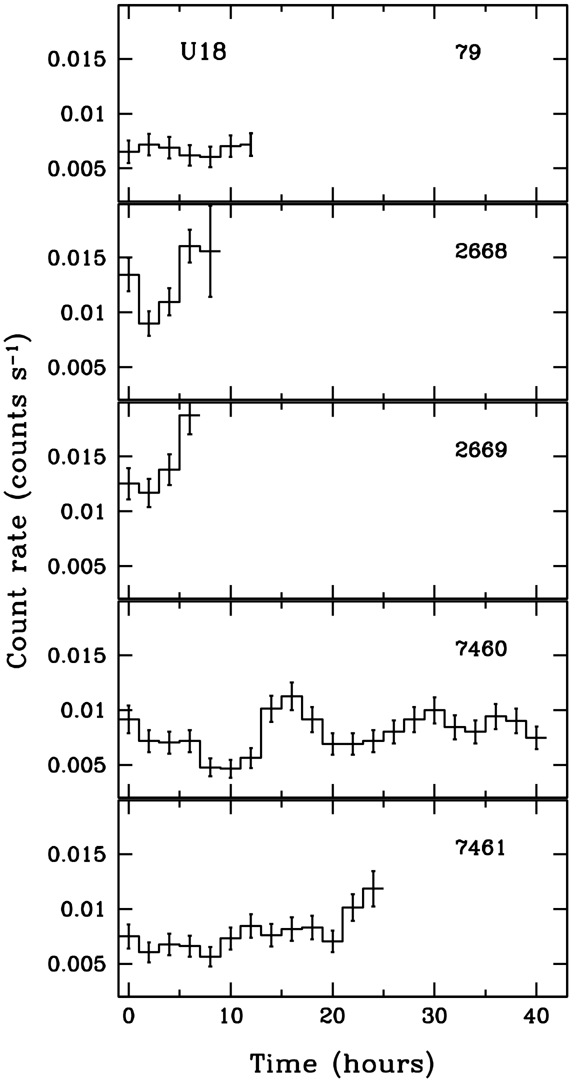

FIG. 5.— X-ray lightcurves of CXOGlb J (U18) in the 0.3–8 keV band from all *Chandra* ACIS observations binned in 1-hour intervals. Time zero corresponds to the start of each observation.

$\sim 10^{31}$ ergs s^{-1} (Stappers et al. 2003; Bogdanov et al. 2005, 2006; Elsner et al. 2008). Moreover, the intrabinary shock in such systems should presumably be visible in X-rays regardless of the pulsar geometry and the orientation of the binary. Therefore, based on our current understanding of the X-ray properties of these sources, *all* MSPs in NGC 6397 should be detected with high significance in the available data.

We have compiled a set of "template" MSP X-ray colors and luminosities using the cluster and field MSPs that have been detected in X-rays to date. These include the 11 MSPs listed in Table 1 of Pavlov et al. (2007), the 15 MSPs in the globular clusters 47 Tuc with unconfused spectra (Bogdanov et al. 2006), one MSP in M71 (Elsner et al. 2008), two MSPs in Ter 5 (Heinke et al. 2006), and the recently discovered PSR J1023+0038 in the field of the Galaxy (Archibald et al. 2009). Using the measured spectral properties of these MSP we calculate their X-ray luminosities and colors as they would appear in NGC 6397 using $N_H = 2 \times 10^{21}$ cm^{-2} and $D = 2.4$ kpc and compare them to the cluster X-ray source population (see Figure 6). We define the color as Xcolor $= 2.5 \log(\mathrm{counts}[0.3 - 1.5\ \mathrm{keV}])/\mathrm{counts}[1.5 - 6\ \mathrm{keV}])$ and consider the absorbed luminosity in the 0.5–6 keV band. To estimate the uncertainties in the derived MSP luminosities, we have considered a nominal 30% error in the pulsar distances plus the uncertainty due to the range of possible distances to NGC 6397. Furthermore, we have taken into account the lack of information regarding the viewing angles of the X-ray-emitting polar caps of any thermal MSPs in NGC 6397 (represented by the dotted lines in Figure 6). High-quality X-ray spectra of nearby thermal MSPs show at least two thermal components and a much fainter hard tail above $\sim$2 keV. For crude photon statistics, the X-ray emission of these MSPs resembles a powerlaw with photon index $\Gamma \sim 2 - 3$ in the 0.5–6 keV range. Thus, to estimate the X-ray luminosities of the sources in NGC 6397 we consider $\Gamma = 2.5$. To ascertain the effect of our choice of spectral model we also used a pure blackbody with $kT = 0.2$ keV and varied $N_{\mathrm{H}} = (1 - 3) \times 10^{21}$ cm^{-1}. We find that the assumptions regarding the spectral shape do not affect the conclusions of our analysis.

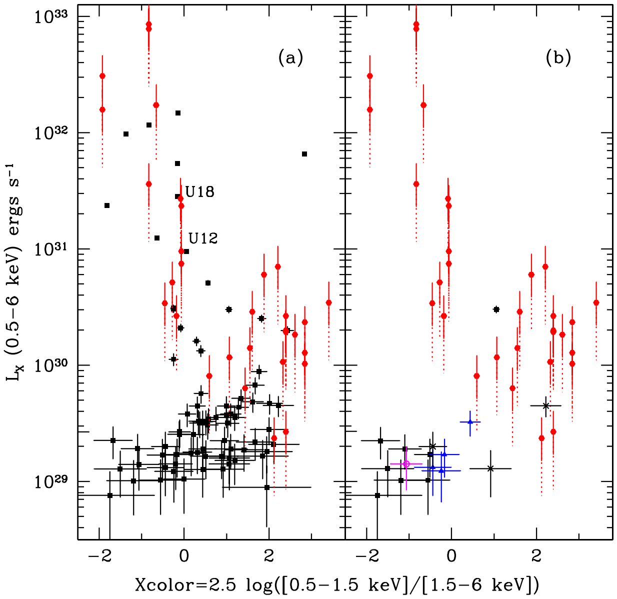

FIG. 6.— (*a*) X-ray luminosity versus color diagram for NGC 6397. The black points show all 79 sources within the NGC 6397 half-mass radius (Table 3), for an assumed powerlaw spectrum with $\Gamma = 2.5$. (*b*) Same as (*a*) but with all sources with probable optical identifications removed. The red circles in both panels correspond to simulated MSPs based on the current Galactic sample of MSPs detected in X-rays (see text for details). Sources with no optical counterparts are marked with black squares, those with ambiguous or unknown optical counterparts with solid blue triangles, the main sequence star candidates with black crosses, and the main-sequence turnoff star candidate with the open magenta circle. The dotted lines extending below the error bars for the MSPs illustrate the effect of the uncertainty in the viewing geometry of the X-ray-emmiting polar caps.

Using the computed set of MSPs, we attempt to identify MSPs in NGC 6397 without the benefit of radio timing searches (see Heinke et al. 2005, for a similar study for 47 Tuc). Important constraints can be gained from optical counterpart identifications using *HST* ACS/WFC observations of the core of NGC 6397

(H. Cohn et al. in preparation). Of the 79 X-ray sources detected within the half-mass radius of NGC 6397, 64 sources have probable associations in the optical (see Table 3) predominantly with active binaries (ABs) and cataclysmic variables (CVs). Additionally, U24 is classified as a qLMXB based on its X-ray properties (Grindlay et al. 2001). The remaining sources either have ambiguous/unknown or no optical counterparts.

Solitary MSPs should have virtually no optical counterparts[12]. Therefore, any X-ray source without an optical counterpart is a viable MSP candidate. Binary MSPs both in clusters and the field are commonly bound to low-mass He white dwarfs or very-low-mass (brown-dwarf-like) companions ($\sim$0.03 $M_\odot$) such as in the canonical "black-widow" system PSR B1957+20 (Fruchter et al. 1988). For NGC 6397, Strickler et al. (2009) have found that none of the 41 He white dwarfs identified optically have X-ray counterparts, implying that they are not partnered with MSPs. The optical properties of black widow systems are not well established as only two objects have been studied in any detail, PSRs B1957+20 (Reynolds et al. 2007) and J2051–0827 (Stappers et al. 2001). Nonetheless, these systems tend to have $L_X \gtrsim 10^{31}$ ergs s^{-1} (Stappers et al. 2003; Bogdanov et al. 2006; Elsner et al. 2008) so the lack of unidentified sources with comparable X-ray luminosities implies the absence of black widow systems in NGC 6397. Moreover, this indicates that aside from J1740–5340 and U18, there are no additional peculiar interacting binaries in this cluster either. Only a single source without an optical counterpart (U113 in Table 3) has X-ray colors and luminosity (Xcolor = 1.05 and $\log L_X = 30.5$) consistent with those of a typical MSP (Figure 6). The sole source with an ambiguous/unknown optical counterpart that has soft colors, U16, as well as U41 and U112, which appears to hav probable main-sequence optical counterparts, are also possible MSP candidates. Based on these findings, we obtain a limit of $\leq$6 MSPs in NGC 6397.

6. DISCUSSION

6.1. *PSR J1740–5340*

Optical observations of the PSR J1740–5340 system (Ferraro et al. 2003; Sabbi et al. 2003) have revealed the presence of ellipsoidal variations as well as a stream of gas protruding from the 1.6 $R_\odot$ secondary star through the L1 point implying that the companion is Roche-lobe overflowing. However, the fact that PSR J1740–5340 is observed as a radio pulsar implies that this gas stream never reaches the underlying NS and is instead swept back and probably expelled from the binary system by the relativistic particle wind from the MSP. The presence of this swept-back gas stream is suggested by the very unusual Hα emission line profile (Sabbi et al. 2003). This gas is likely the cause for the irregular radio eclipses the MSP exhibits over a wide range of orbital phases.

As seen in "black-widow" systems (Stappers et al. 2003; Bogdanov et al. 2006; Elsner et al. 2008) and "exchanged" MSP systems (Bogdanov et al. 2005) the interaction between the pulsar wind and material from the companion star should result in a shock front where the ram pressure of the wind balances the pressure of the infalling gas leading to X-ray emission due to particle acceleration (Arons & Tavani 1993). In this scenario, synchrotron emission is expected to be the primary energy loss mechanism in the resulting shock wave, given that it occurs in a relatively strong magnetic field. In the PSR J1740–5340 binary, for a shock situated approximately at the L1 point and an isotropic pulsar wind, the pulsar magnetic field at this distance ($\approx 4 \times 10^{11}$ cm) immediately upstream from the shock is $B_1 \approx 2 - 3$ G or $B_1 \approx 0.1$ G , implying a post-shock field of $B_2 = 3B_1 \sim 6 - 9$ G or $B_2 \sim 0.3$ G (Arons & Tavani 1993). The two values correspond to the two possible cases of a magnetically dominated shock ($\sigma \gg 1$, where σ is the magnetic to kinetic energy flux ratio) or a kinetic energy dominated shock ($\sigma = 0.003$ as in the Crab pulsar). This implies that the X-ray emission from PSR J1740–5340 source is most likely non-thermal in origin and not from a thermal plasma.

An intrabinary shock origin of the X-rays from J1740–5340 is also suggested by the fact that the derived spectral parameters are quite similar to those of the canonical "black-widow" pulsar, PSR B1957+20 (Stappers et al. 2003), the peculiar MSP-main-sequence binary in 47 Tuc, PSR J0024–7204W (Edmonds et al. 2002; Bogdanov et al. 2005), and the recently identified radio MSP in the field of the Galaxy, PSR J1023+0038 (Archibald et al. 2009, and references therein), which also appears to be bound to a non-degenerate ("main-sequence-like") star. Moreover, the shape of the X-ray modulations at the binary period are quite similar to that of J0024–7204W (see Figure 1 in Bogdanov et al. 2005). This variability can be attributed to an occultation of the shocked material by the secondary star. This scenario is supported by the compelling (albeit marginal) evidence for a softening of the spectrum at $\phi \approx 0.25$. The constraint on the system inclination ($47^\circ - 56^\circ$ Ferraro et al. 2003) suggests that the line of sight to the pulsar is never obstructed by the companion. Therefore, when the shock is occulted at $\phi \approx 0.25$ (either partially or totally), the soft thermal radiation from the MSP surface provides a larger contribution to the total X-ray emission, resulting in a softening of the observed spectrum. In principle, detailed orbital-phase-resolved X-ray observations would permit disentanglement of the thermal polar cap emission and the non-thermal shock emission.

Note that the moderate spin-down luminosity[13] of $\dot{E} \approx 3.3 \times 10^{34}$ ergs s^{-1} (Bassa & Stappers 2004) does not favor a magnetospheric origin of the observed non-thermal X-rays considering that most other MSPs with comparable values of $\dot{E}$ exhibit much softer, predominantly thermal spectra (see, e.g., Bogdanov et al. 2006; Zavlin 2006; Bogdanov & Grindlay 2009). Furthermore, for pulsed non-thermal emission, it is difficult to explain the observed variations in the total flux and the softening of the spectrum at $\phi \approx 0.25$.

6.2. *U18: A Hidden MSP?*

---

[12] The current best limits on optical emission from isolated MSPs come from observations of the nearby PSRs J0030+0451 ($D \approx 300$ pc) and J2124–3358 ($D \approx 270$ pc), for which no counterparts are found down to B, V, and R magnitudes of 27 − 28 (Koptsevich et al. 2003; Mignani & Becker 2004).

[13] As discussed by D'Amico et al. (2001), the effect of cluster acceleration on the measured pulsar spindown rate is neglegible.

The X-ray and optical properties of U18 are consistent with those of a binary containing a rotation-powered pulsar wind interacting with material from the secondary star. It is interesting to note the significantly larger luminosity compared to J1740–5340 and other interacting MSP systems. This could indicate either a much larger shock region, an enhanced density of radiating particles, and/or a more energetic pulsar wind. If this binary does indeed harbor a MSP, it may be difficult to detect at radio frequencies due to the large quantities of gas present within and around the binary. This gas may render the pulsar perpetually eclipsed at radio frequencies. Thus, U18 may belong to the class of so-called "hidden" MSPs (Tavani 1991) making a confirmation of its true nature quite difficult. The detection of pulsed X-ray emission from the pulsar itself may also be difficult due to the dominant X-ray flux from the intrabinary shock and the *a priori* unknown pulsar spin period.

We note that, at present, we cannot strictly rule out the possibility that U18 is a cataclysmic variable, such as an intermediate polar (IP), instead of an MSP. These objects also generally exhibit hard X-ray spectra and X-ray luminosities comparable to that of U18. In addition, the IP AKO9 in 47 Tuc (Heinke et al. 2005) appears to have a "red straggler" or "sub-subgiant" companion as well. In order to unveil the true nature of the U18 system, further optical observations, optimized for variability study, are needed. The cadence of our *HST* ACS/WFC optical dataset (10 single-orbit observations spaced ∼1 month apart, see H. Cohn et al. 2009, in preparation) is not suitable for a reliable determination of the binary period of this system.

6.3. *The Millisecond Pulsar Population of NGC 6397*

The analysis in §5 suggests that NGC 6397 most likely harbors $1 - 6$ MSPs. It is of interest to compare these limits to the expected number of MSPs in this cluster, scaling by the stellar encounter rate (Γ, Verbunt & Hut 1987) from other clusters with detected MSPs[14]. Pooley et al. (2003) integrate collision rates over King models out to the half-mass radius, finding a collision rate for NGC 6397 1/74 that of 47 Tuc. Other analyses (e.g. Heinke et al. 2003; Bassa et al. 2008), using a simpler formalism ($\Gamma = \rho_0^{1.5} r_c^2$, where ρ_0 is the central density and r_c is the core radius of the cluster), find collision rates for NGC 6397 roughly 1/10 that of 47 Tuc. As 47 Tuc has 23 known MSPs, and has been suggested to have a total of ∼25 MSPs (Heinke et al. 2005), the two approaches suggest either < 1 or ∼2 MSPs should be present in NGC 6397. Comparisons with the number of MSPs in other clusters, such as Terzan 5 (Ransom et al. 2005) give similar results. However, Γ comparisons seem to underpredict the number of X-ray sources in NGC 6397 (Pooley et al. 2003), indicating differences in the X-ray binary production processes in core-collapsed clusters such as NGC 6397. For instance, Fregeau (2008) has suggested that continuing globular cluster collapse means that the values of Γ of King-model clusters during the epoch of X-ray binary formation were a factor of 3 smaller. In any case, the predicted numbers of MSPs in NGC 6397 from any of the above comparisons are generally in agreement with our estimate of $1 - 6$ MSPs in NGC 6397.

7. CONCLUSION

We have presented *Chandra X-ray Observatory* ACIS-S observations of the nearby core-collapsed globular cluster NGC 6397. The depth of the available data has allowed interesting insight into the MSP population of this cluster. For instance, it has provided a more complete multi-wavelength picture of the PSR J1740–5340 binary. This peculiar system appears to exhibit predominantly non-thermal emission modulated at the orbital phase. Given the pulsar energetics, the variable non-thermal X-ray emission is indicative of interaction between the relativistic pulsar wind and material from the companion, with evidence for an occultation of the resulting shock by the secondary star. Ascertaining the detailed geometry of the intrabinary shock would require much more sensitive orbital-phase resolved spectroscopic X-ray and optical observations of this system than presently available.

Based on its X-ray and optical properties, U18 is a strong candidate for a MSP, though one that may be perpetually eclipsed at radio frequencies. As noted by Tavani (1991) such MSPs may be relatively common both in globular clusters and in the field of Galaxy. Moreover, these sources may be mis-classified as LMXBs or CVs based on their X-ray to optical flux ratio alone (see in particular Homer et al. 2006; Archibald et al. 2009). Further detailed multi-wavelength observations of PSR J1740–5340, U18, and similar systems may reveal more information concerning the physics of the shock, which, may, in principle offer insight into the properties of MSP winds, collisionless relativistic shocks, and particle acceleration mechanisms. Moreover, this and similar MSP binaries provide important clues about the behavior of accreting neutron stars transitioning to rotation power, which are believed to also contain an active radio pulsar and an overflowing companion (Campana et al. 2004; Heinke et al. 2007, 2009).

The deep X-ray observations of NGC 6397 supplemented by optical observations, also provide insight into the MSP population of this cluster. Specifically, if the X-ray luminosity function of the NGC 6397 MSP population resembles that of the Galactic sample of MSPs, then this cluster contains no more than ∼6 MSPs. This range of values is generally consistent with those inferred based on scaling of stellar encounter rates in globular clusters.

This work was funded in part by NASA *Chandra* grant GO7-8033A, awarded through the Harvard College Observatory. S. B. is supported in part by a Canadian Institute for Advanced Research Junior Fellowship. The research in this paper has made use of the NASA Astrophysics Data System (ADS).

---

[14] We note that the numbers of (quiescent) LMXBs in globular clusters, likely progenitors of MSPs, appear to scale with Γ (Pooley & Hut 2006; Heinke et al. 2006).

REFERENCES

Archibald, A. M., et al. 2009, Science, 324, 1411

Arons, J. & Tavani M. 1993, ApJ, 403, 249

Bassa, C. G., Pooley, D., Homer, L., Verbunt, F., Gaensler, B. M., Lewin, W. H. G., Anderson, S. F., Margon, B., Kaspi, V. M., & van der Klis, M. 2004, ApJ, 609, 755
Bassa, C. G. & Stappers, B. W. 2004, A&A, 425, 1143
Bassa, C. G., Pooley, D., Verbunt, F., Homer, L., Anderson, S. F., & Lewin, W. H. G. 2008, A&A, 488, 921
Becker, W., Swartz, D. A., Pavlov, G. G., Elsner, R. F., Grindlay, J. E., Mignani, R., Tennant, A. F., Backer, D., Pulone, L., Testa, V., & Weisskopf, M. C. 2003, ApJ, 594, 798
Bhattacharya, D. & van den Heuvel, E. P. J. 1991, Phys. Rep. 203, 1
Bogdanov, S., Grindlay, J. E., & van den Berg, M. 2005, ApJ, 630, 1029
Bogdanov, S., Grindlay, J. E., Heinke, C. O., Camilo, F., Freire, P. C. C, & Becker, W. 2006, ApJ, 646, 1104
Bogdanov, S. & Grindlay, J. E. 2008, AIPC, 983, 64
Bogdanov, S., Grindlay, J. E., & Rybicki, G. B. 2008, ApJ, 689, 407
Bogdanov, S. & Grindlay, J. .E. 2009, ApJ, 703, 1557
Burderi, L., D'Antona, F., & Burgay, M. 2002, ApJ, 574, 325
Camilo, F., Lorimer, D. R., Freire, P., Lyne, A. G., & Manchester, R. N. 2000, ApJ, 535, 975
Camilo. F. & Rasio, F. A. 2005, ASP Conf. Ser. Vol. 328: Binary Radio Pulsars, eds. F. A. Rasio & I. H. Stairs (San Francisco: ASP), p. 147
Campana, S., D'Avanzo. P., Casares, J., Covino, S., Israel, G. L., Marconi, G., Hynes, R., Charles, P., & Stella, L. 2004, ApJ, 614, L49
Castilho, B. V., Pasquini, L., Allen, D. M., Barbuy, B., Molaro, P. 2000, A&A, 361, 92
Damiani, F., Maggio, A., Micela, G., & Sciortino, S. 1997a, ApJ, 483, 350
Damiani, F., Maggio, A., Micela, G., & Sciortino, S. 1997b, ApJ, 483, 370
D'Amico, N., Lyne, A. G., Manchester, R. N., Possenti, A., & Camilo, F. 2001, ApJ, 548, L171
D'Amico, N., Possenti, A., Fici, L., Manchester, R. N., Lyne, A. G., Camilo, F., & Sarkissian, J. 2002, ApJ, 570, L89
Edmonds, P. D., Gilliland, R. L., Camilo, F., Heinke, C. O., & Grindlay, J. E. 2002, ApJ, 579, 741
Elsner, R. F., et al. 2008, ApJ, 687, 1019
Ferraro, F. R., Sabbi, E., Gratton, R., Possenti, A., D'Amico, N., Bragaglia, A., & Camilo, F. 2003, ApJ, 584, 2003
Fregeau, J. M. 2008, ApJ, 673, 25
Freire, P. C., Camilo, F., Kramer, M., Lorimer, D. R., Lyne, A. G., Manchester, R. N., & D' Amico, N. 2003, MNRAS, 340, 1359
Fruchter, A. S., Stinebring, D. R., & Taylor, J. H. 1988, Nature, 333, 237
Gratton, R. G., et al. 2001, A&A, 369, 87
Grindlay, J. E., Heinke, C. O., Edmonds, P. D., Murray, S. S., Cool, A. M. 2001, ApJ, 563, L53
Grindlay, J. E., Camilo, F., Heinke, C. O., Edmonds, P. D., Cohn, H., & Lugger, P. 2002, ApJ, 581, 470
Grindlay, J. E. 2005, AIPC, 797, 13
Hansen, B. M. S., et al. 2007, ApJ, 671, 380
Heinke, C. O., Grindlay, J. E., Lugger, P. M., Cohn, H. N., Edmonds, P. D., Lloyd, D. A., Cool, A. M. 2003, 598, 501
Heinke, C. O., Grindlay, J. E., Edmonds, P. D., Cohn, H. N., Lugger, P. M., Camilo, F., Bogdanov, S., & Freire, P. C. 2004, ApJ, 625, 796
Heinke, C. O., Wijnands, R., Cohn, H. N., Lugger, P. M., Grindlay, J. E., Pooley, D., & Lewin, W. H. G. 2006, ApJ, 651, 1098
Heinke, C. O., Jonker, P. G., Wijnands, R., Taam, R. E. 2007, ApJ, 660, 1424
Heinke, C. O., Jonker, P. G., Wijnands, R., Deloye, C. J., Taam, R. E. 2009, ApJ, 691, 1035
Homer, L., et al. 2006, AJ, 131, 562
Hong, J., van den Berg, M., Schlegel, E. M., Grindlay, J. E., Koenig, X., Laycock, S., & Zhao, P. 2005, ApJ, 635, 907
Hui, C. Y. & Becker, W. 2006, A&A, 448, L13
Kaluzny, J., Thompson, I. B., Krzeminski, W., & Schwarzenberg-Czerny, A. 2006, MNRAS, 365, 548
Koptsevich, A. B., Lundqvist, P., Serafimovich, N. I., Shibanov, Yu. A., & Sollerman, J. 2003, A&A, 400, 265
Mignani, R. P. & Becker, W. 2004, AdSpR, 33, 616
Orosz, J. A. & van Kerkwijk, M. H. 2003, A&A, 397, 237
Pavlov, G. G., Kargaltsev, O., Garmire, G. P., & Wolszczan, A. 2007, ApJ, 664, 1072
Pooley, D., et al. 2003, ApJ, 591, L131
Pooley, D., Hut, P. 2006, ApJ, 646, L143
Ransom, S. M., Hessels, J. W. T., Stairs, I. H., Freire, P. C. C., Camilo, F., Kaspi, V. M., Kaplan, D. L. 2005, Science, 307, 892
Reynolds, M. T., Callanan, P. J., Fruchter, A. S., Torres, M. A. P., Beer, M. E., & Gibbons, R. A. 2007, MNRAS, 379, 1117
Rutledge, R. E., Fox, D. W., Kulkarni, S. R., Jacoby, B. A., Cognard, I., Backer, D. C., & Murray, S. S. 2004, ApJ, 613, 522
Sabbi, E., Gratton, R., Ferraro, F. R., Bragaglia, A., Possenti, A., D'Amico, N., & Camilo, F. 2003, ApJ, 589, L41
Stappers, B. W., van Kerkwijk, M. H., Bell, J. F., & Kulkarni, S. R. 2001, 548, L183
Stappers, B. W., Gaensler, B. M., Kaspi, V. M., van der Klis, M., & Lewin, W. H. G. 2003, Science, 299, 1372
Strickler, R. R., Cool, A. M., Anderson, J., Cohn, H. N., Lugger, P. M., & Serenelli, A. M. 2009, ApJ, 699, 40
Tavani, M. 1991, ApJ, 379, L69
Verbunt, F. & Hut, P. 1987, IAUS, 125, 187
Zavlin, V. E. 2006, ApJ, 638, 951
Zavlin, V. E. 2007, Ap&SS, 308, 297

TABLE 3
X-ray Sources in NGC 6397

U Name[a] (1)	CXOGlb J Name (2)	α (J2000.0)[b] (3)	δ (J2000.0)[b] (4)	$r_{95\%}$ ($''$)[c] (5)	Soft Counts[d] (0.5–1.5 keV) (6)	Hard Counts[d] (1.5–6 keV) (7)	Flux[e] (0.5–6 keV) (8)	ID Type[f]
5	174054.5–534044	17 40 54.531	–53 40 44.57	0.33	167	31	41.7	AB?
7	174052.8–534121	17 40 52.832	–53 41 21.77	0.32	252	150	84.6	CV
10	174048.9–533948	17 40 48.978	–53 39 48.62	0.29	283	1504	390.8	CV
11	174045.7–534041	17 40 45.781	–53 40 41.52	0.32	72	55	26.7	CV
12	174044.6–534041	17 40 44.621	–53 40 41.60	0.30	382	363	157.3	MSP
13	174044.0–534039	17 40 44.084	–53 40 39.17	0.31	107	135	51.4	CV
14	174043.3–534155	17 40 43.328	–53 41 55.46	0.40	17	10	5.7	AB
15	174042.9–534033	17 40 42.910	–53 40 33.81	0.34	42	9	11.2	AB
16	174042.6–534215	17 40 42.636	–53 42 15.24	0.42	15	10	5.4	?
17	174042.6–534019	17 40 42.651	–53 40 19.30	0.28	5358	6114	2458.0	CV
18	174042.6–534027	17 40 42.606	–53 40 27.62	0.29	995	1142	470.2	MSP?
19	174042.3–534028	17 40 42.306	–53 40 28.70	0.28	2777	5934	1927.3	CV
21	174041.8–534021	17 40 41.830	–53 40 21.37	0.29	1974	2279	901.4	CV
22	174041.7–534029	17 40 41.701	–53 40 29.00	0.31	104	131	50.3	CV
23	174041.5–534019	17 40 41.597	–53 40 19.30	0.28	1677	5915	1609.5	CV
24	174041.4–534004	17 40 41.468	–53 40 04.43	0.28	4797	353	1088.8	qLMXB
25	174041.2–534025	17 40 41.237	–53 40 25.79	0.33	39	49	18.7	CV?
28	174038.9–533951	17 40 38.904	–53 39 51.09	0.30	351	629	206.1	GLX
31	174034.2–534115	17 40 34.202	–53 41 15.28	0.37	26	18	9.5	CV
41	174045.0–533955	17 40 45.008	–53 39 55.21	0.36	31	4	7.5	MS?
42	174043.0–533831	17 40 43.059	–53 38 31.29	0.34	141	15	33.0	AB
43	174040.5–534022	17 40 40.543	–53 40 22.79	0.36	25	10	7.4	AB
60	174047.8–534128	17 40 47.807	–53 41 28.40	0.41	10	11	4.4	CV

TABLE 3
X-ray Sources in NGC 6397

61	174045.2–534028	17 40 45.223	–53 40 28.60	0.32	79	85	34.8	CV?
62	174030.4–533917	17 40 30.422	–53 39 17.47	0.48	12	5	3.7	AB?
63	174031.6–533846	17 40 31.663	–53 38 46.36	0.42	31	7	8.0	AB?
65	174037.5–533917	17 40 37.558	–53 39 17.85	0.43	14	3	3.6	AB?
66	174038.9–533849	17 40 38.918	–53 38 49.80	0.48	9	4	2.7	AB?
67	174040.0–534016	17 40 40.065	–53 40 16.59	0.41	8	6	3.0	AB
68	174040.7–533832	17 40 40.730	–53 38 32.63	0.44	1	20	4.4	?
69	174040.8–534017	17 40 40.867	–53 40 17.17	0.37	15	9	5.1	AB
70	174041.6–534033	17 40 41.693	–53 40 33.33	0.32	59	41	22.1	AB
73	174042.6–533928	17 40 42.681	–53 39 28.73	0.38	22	8	6.3	AB
75	174043.6–534030	17 40 43.666	–53 40 30.61	0.39	9	10	4.2	AB
76	174043.8–534116	17 40 43.818	–53 41 16.32	0.38	21	7	5.9	AB
77	174044.1–534211	17 40 44.125	–53 42 11.48	0.42	18	7	5.2	AB?
79	174046.4–534004	17 40 46.409	–53 40 04.05	0.38	18	9	5.9	AB
80	174046.4–534156	17 40 46.455	–53 41 56.50	0.39	20	15	7.4	CV?
81	174046.4–534115	17 40 46.481	–53 41 15.44	0.38	15	11	5.5	AB
82	174048.5–533939	17 40 48.537	–53 39 39.53	0.37	31	9	8.6	AB
83	174049.6–534043	17 40 49.615	–53 40 43.02	0.46	5	6	2.4	CV?
84	174054.8–534019	17 40 54.807	–53 40 19.79	0.40	32	5	7.8	AB?
86	174037.4–534147	17 40 37.473	–53 41 47.24	0.35	56	11	14.6	AB?
87	174042.8–534026	17 40 42.877	–53 40 26.45	0.37	14	10	5.3	AB
88	174042.8–534023	17 40 42.863	–53 40 23.43	0.37	20	8	6.2	AB
89	174043.6–534024	17 40 43.613	–53 40 24.60	0.41	11	3	3.1	AB
90	174041.7–534014	17 40 41.779	–53 40 14.42	0.36	26	8	7.2	AB
91	174042.4–534041	17 40 42.430	–53 40 41.65	0.40	6	9	3.3	MS
92	174043.9–534035	17 40 43.916	–53 40 35.39	0.40	11	4	3.2	AB?
93	174042.3–534046	17 40 42.393	–53 40 46.62	0.42	6	7	2.8	?
94	174042.8–534049	17 40 42.868	–53 40 49.07	0.40	14	2	3.4	AB
95	174040.3–534044	17 40 40.320	–53 40 44.58	0.47	4	4	1.7	AB?
96	174039.0–534023	17 40 39.097	–53 40 23.09	0.42	11	2	2.7	AB
97	174043.9–534005	17 40 43.918	–53 40 05.90	0.44	4	6	2.2	?
98	174040.9–534058	17 40 40.994	–53 40 58.40	0.41	12	2	3.0	AB
99	174046.4–534030	17 40 46.431	–53 40 30.40	0.50	6	1	1.5	AB
100	174038.2–534046	17 40 38.201	–53 40 46.55	0.45	6	4	2.1	AB
101	174045.3–534101	17 40 45.399	–53 41 01.40	0.39	19	3	4.6	AB?
102	174038.8–533943	17 40 38.845	–53 39 43.12	0.40	11	9	4.2	AB
103	174035.6–534012	17 40 35.698	–53 40 12.56	0.44	9	3	2.5	AB
104	174043.1–533929	17 40 43.124	–53 39 29.04	0.44	5	8	2.8	none
105	174036.5–534107	17 40 36.521	–53 41 07.85	0.44	8	5	2.7	AB
106	174043.7–533917	17 40 43.737	–53 39 17.52	0.51	3	5	1.7	none
107	174034.1–534017	17 40 34.115	–53 40 17.01	0.39	16	10	5.4	AB
108	174052.0–533948	17 40 52.099	–53 39 48.25	0.46	9	6	3.2	GLX?
109	174052.7–534052	17 40 52.728	–53 40 52.88	0.50	8	3	2.3	AB?
110	174033.4–533916	17 40 33.455	–53 39 16.83	0.50	8	3	2.6	AB
111	174029.8–534026	17 40 29.845	–53 40 26.99	0.45	3	14	3.7	none
112	174050.3–533906	17 40 50.374	–53 39 06.00	0.53	7	3	2.1	MS
113	174042.7–534020	17 40 42.764	–53 40 20.76	0.31	161	61	50.0	none
114	174043.4–534034	17 40 43.469	–53 40 34.34	0.45	4	5	2.0	?
116	174042.2–534019	17 40 42.236	–53 40 19.97	0.36	15	14	6.3	AB
117	174042.1–534025	17 40 42.153	–53 40 25.56	0.41	7	6	2.9	AB
118	174041.5–534015	17 40 41.576	–53 40 15.88	0.43	3	8	2.3	MSTO
119	174041.2–534019	17 40 41.261	–53 40 19.35	0.40	4	11	3.2	none
120	174046.5–534015	17 40 46.517	–53 40 15.64	0.53	6	0	1.3	AB?
121	174033.6–533934	17 40 33.631	–53 39 34.96	0.50	2	8	2.1	none
122	174047.9–533924	17 40 47.903	–53 39 24.83	0.58	1	5	1.3	none
123	174049.6–533845	17 40 49.621	–53 38 45.93	0.60	2	6	1.7	none

---

[a] Source names based on the X-ray source list from Grindlay et al. (2001).

[b] J2000.0 `acis_extract` derived positions of each source boresighted to the frame of the *HST* ACS dataset.

[c] The 95% positional uncertainty radius based on Hong et al. (2005), in units of arcseconds.

[d] Background-subtracted source counts in the 0.3–1.5 and 1.5–6 keV bands.

[e] Source flux in the 0.5–6 keV band in units of 10^{-16} ergs cm^{-2} s^{-1} assuming a power-law model with spectral photon index $\Gamma = 2.5$.

[f] Probable source identifications based on optical counterpart properties (from H. Cohn et al., in preparation). AB is an active binary, CV a cataclysmic variable, GLX a background galaxy, qLMXB a quiescent low mass X-ray binary, MS a main sequence star, MSTO a main sequence turn-off star, and MSP a millisecond pulsar. Sources marked with an additional "?" are probable but less certain classifications, those with only "?" have ambiguous or unknown, and those labeled "none" have no optical counterparts.